

Article

# Evanescent-Field Excited Surface Plasmon-Enhanced U-Bent Fiber Probes Coated with Au and ZnO Nanoparticles for Humidity Detection

Elnaz Afsharipour <sup>1,2,\*</sup>, Kirtiman Deo Malviya <sup>1</sup>, Mohammadreza Montazeri <sup>2</sup>, Ebrahim Mortazy <sup>2</sup>, Ramin Soltanzadeh <sup>2</sup>, Alireza Hassani <sup>2</sup>, Federico Rosei <sup>1</sup>  and Mohamed Chaker <sup>1</sup>

<sup>1</sup> Institut National de la Recherche Scientifique INRS-Energie, Materiaux et Telecommunications, 1650, Blvd. Lionel-Boulet, Varennes, QC J3X 1S2, Canada

<sup>2</sup> Maxwellian Inc., 3 Place Ville Marie, Montreal, QC H3B 2E3, Canada

\* Correspondence: e.afsharipour@gmail.com

**Abstract:** We report the design, fabrication, and testing of a humidity sensor based on an optical fiber-based evanescent wave probe. The fiber was bent into a U-shape and de-cladded at the location of the bending. The de-cladded section was coated either with Au or with ZnO nanoparticles. Humidity is detected based on the interaction in the surface plasmon resonance of the Au/ZnO nanoparticles excited by an evanescent wave of light passing through the optical fiber. The response of the U-bent fibers to humidity was investigated using a specifically designed low-voltage portable interrogation box. We found that the fibers coated with ZnO nanoparticles were able to detect a minimum 0.1% change in humidity with an average sensitivity of  $143 \mu\text{V}/\%\text{RH}$  and 95% linearity over the 10% to 80% humidity range. In comparison, samples coated with Au and Au + ZnO nanoparticles demonstrated a minimum change detection of 0.3% RH and 2% RH respectively. The response and recovery time of the sensor were measured to be 3 s and 4 s, respectively, for a 60% change in humidity from 20% to 80%. The entire measurement system was operated by consuming an electrical power of 1.62 W at an input voltage of 12 Vdc.



**Citation:** Afsharipour, E.; Malviya, K.D.; Montazeri, M.; Mortazy, E.; Soltanzadeh, R.; Hassani, A.; Rosei, F.; Chaker, M. Evanescent-Field Excited Surface Plasmon-Enhanced U-Bent Fiber Probes Coated with Au and ZnO Nanoparticles for Humidity Detection. *Processes* **2023**, *11*, 642. <https://doi.org/10.3390/pr11020642>

Academic Editors: Gugu Hlengiwe Mhlongo and Dimitra Papadaki

Received: 27 December 2022

Revised: 6 February 2023

Accepted: 15 February 2023

Published: 20 February 2023



**Copyright:** © 2023 by the authors. Licensee MDPI, Basel, Switzerland. This article is an open access article distributed under the terms and conditions of the Creative Commons Attribution (CC BY) license (<https://creativecommons.org/licenses/by/4.0/>).

## 1. Introduction

Precise measurements of humidity are essential in a variety of applications such as microbiological experiments [1], pharmaceutical product development [2], the processed-food industry [3], and automated agricultural processes [4]. The applicability and importance of accurate measurements of moisture have prompted increased research efforts on humidity sensors. Several sensing approaches including chemical-based, electronic-based [5–8], mechanical-based, and optics-based probes have been employed to fabricate humidity measurement devices [9]. Among these, optics-based humidity sensors have been shown to have a fast response time while being stable against electromagnetic interference noise. Response times of 10 ms and 30 ms have been reported in [10–12]. Optical fiber-based humidity sensors have the advantages of integrability and ease of fabrication. Optical fiber-based sensors can be categorized into four general groups, specifically, absorbance-based, Fiber Bragg Gratings (FBG), interferometric, and evanescent wave-based sensors [13,14]. In absorbance-based sensors, the interaction of water molecules and some chemical reagents affects the intensity of light passing through the fiber [15,16]. FBG humidity sensors typically use a moisture-sensitive polymer that stretches when exposed to humidity [17–19]. This stretch applies a strain to the grating which results in a change in its resonant Bragg wavelength. Interference-based sensors employ two light beams that propagate through two different paths of optical fibers, with one of the fibers exposed to humidity [20]. The

humidity is then measured by monitoring the change in the optical power amplitude due to the interference between the two light beams. In two of the three methods mentioned above, the humidity is converted to a mechanical change in the material. One disadvantage of these methods is that the absorption and desorption happen at different speeds, which causes a different response time relative to the rise and fall of the detected humidity. However, the sensing mechanism in evanescent wave-based sensors is based on the interaction between the humidity and the exponentially decaying field surrounding the cladding region [21,22]. Therefore, in this method, no mechanical property of the material is changing due to the humidity, which makes it more stable over time. To allow the evanescent wave to penetrate the experimental medium, the optical fiber is partially unclad. The penetration depth of the evanescent wave can be increased by bending the fiber to form a U shape [23]. Although in harsh environments this method can suffer from sensitivity reduction due to the contamination of the optical fiber, it is worth exploring because of its high initial sensitivity and response time. In the following section, the theory and functionality of evanescent wave sensors are further explored.

## 2. Principle of Operation of Evanescent Wave Sensor

When light passes through the core of an optical fiber, the vicinity of the optical fiber is surrounded by a near-field electromagnetic standing wave, whose intensity decays exponentially along the distance to the fiber core. The working principle of evanescent wave sensors is based on the interaction of this field with the quantity to be measured, which, in the present case, is humidity.

When the fiber is bent, the majority of the light's power is transferred from the guided mode to the leaky mode, which intensifies the amplitude of the evanescent wave. In the guided light mode, the energy profile of the mode is confined to the fiber core and transferred through the fiber with minimum loss. A leaky mode is a mode that is not confined to the fiber core, so its energy leaks to the cladding. By removing the cladding of the fiber, the core of the optical fiber is exposed to the surrounding environment, which then acts as the cladding of the optical fiber. Therefore, the evanescent field that extends from the fiber core to the surrounding environment, interacts with the water molecules in the unclad region. The interaction of the evanescent wave with the water molecules affects the intensity of the light that passes through the optical fiber's core. This change in the light's intensity can be explained by the fact that the refractive index of the cladding changes in the presence of the water molecules. A larger change in the intensity of the light passing through the fiber core corresponds to a greater sensitivity for humidity detection. The change in the light's intensity can be amplified by coating the unclad part of the fiber with some reagents that have a stronger interaction with the particle to be detected (in this case, water molecules).

When the fiber is coated with gold nanoparticles (AuNp), the evanescent field can cause an oscillation in the conduction electrons at the surface between the fiber core and the nanoparticles layer, which excites the surface plasmon polariton. The propagation of the surface plasmon polariton depends on the refractive index of the interface medium. The refractive index of the interface medium can change when a particle is attached to the core surface, which results in a change in the propagation of the surface plasmon polaritons. This change can be detected by monitoring the transmission of light through the fiber. This property allows the accurate detection of different particles [24–27]. The localized surface plasmon effect has also been observed in ZnO nanoparticles and thin films [28,29].

Unclad fibers have also been coated with various particles to improve the optical probe's response to water molecules. Polyvinyl alcohol (PVA) [21,30], CoCl<sub>2</sub> [21], silica gel/Methylene Blue [31], agarose [32], Sol-gel/TiO<sub>2</sub> film [33], MgO film [34], Ag-Polyaniline nanocomposite [35], phenol red doped PMMA [36], polyaniline with Co nanoparticles [37], and ITO [38] have been used to amplify the sensitivity of the sensor to humidity.

In addition to water molecules, "U-bent" fibers coated with different materials have also been employed to detect other substances. Some examples include analysis of ethanol,

methanol, and acetone water mixtures using U-bent probes [39–43], detection of dissolved oxygen using sol-gel/Ru coating [44], and detection of immunoglobulin using protein/antibody/AuNp coated probes [24].

Our objective is to develop a fiber-optics-based sensor that is highly sensitive to humidity changes of less than 1%. In addition, we aim to obtain a fast response time and linear output. The developed sensing system, including a laser diode, photodetector, and all the driving electronics are designed to be portable and of low-power-consumption. To fabricate the humidity probes, de-cladded U-bent fibers were coated with Au, ZnO, and Au/ZnO thin film and nanoparticles as sensing agents to amplify the sensitivity. The fabricated fiber-optic sensors were then used to measure humidity in a controlled setup. A comprehensive study of the sensing ability of the optical fiber probes was performed to evaluate the efficiency of the thin films and nanoparticles in measuring humidity. The experimental details and results are discussed in the following sections.

### 3. Materials and Methods

Fabrication of the probes was performed in three steps, as described in the following sections.

#### 3.1. U-Bent Fiber Fabrication

The selected fiber was made of a pure silica core and TECS (Technology Enhanced Clad Silica) hard cladding with a core diameter of 600  $\mu\text{m}$  and a cladding diameter of 630  $\mu\text{m}$ . The core's refractive index was 1.458 and the cladding's refractive index was 1.398. Fibers were bent using a semi-automatic fiber bending machine that was developed at Maxwellian Inc (Montreal, QC, Canada), specifically for symmetrical bending of the fibers with minimal mechanical stress. A bending radius of 5 mm was selected, based on previously reported studies [21,33]. The TECS cladding of the fiber was also removed when the fiber was exposed to the flame during the bending process. The two ends of the fibers were cut on their crystal plane using a diamond pen and polished on the fiber optic polishing pads of 9  $\mu\text{m}$ , 5  $\mu\text{m}$ , and 1  $\mu\text{m}$  grit size, respectively. The fiber ends were washed with isopropanol alcohol before the measurements.

#### 3.2. Nanoparticle Coating Using the Pulsed-Laser Ablation in Liquid (PLAL) Method

The uncladded section of the U-bent optical fibers was first sonicated for 10 min in acetone and 10 min in isopropanol followed by 60 min in Nanostrip solution, which is a stabilized formulation of sulfuric acid and hydrogen peroxide. The fibers were then rinsed with hot and room-temperature water several times to remove any residues of the Nanostrip and dried in nitrogen gas flow. The fibers were then annealed in a furnace at a temperature of 120 °C for an hour to produce the (-OH) group at the surface of the fiber.

The (-OH) group-activated fibers were then functionalized with (3-aminopropyl) trimethoxysilane (APTMS). The functionalizing process started with immersing the fibers in a 10% (*v/v*) solution of APTMS in isopropanol for one hour at 50 °C. The functionalized optical fibers were rinsed with isopropanol and DI water to remove the unbounded APTMS. The optical fibers were annealed at 120 °C for one hour to cure and strengthen the bonds with the silica fiber.

Pulsed laser ablation in liquid (PLAL) was used to synthesize the nanoparticles. In this method, a target made of a solid disk of either gold or ZnO is placed at the bottom of a container filled with de-ionized water. The pulsed laser light, coming from a KrF excimer laser, of 248 nm wavelength and pulse duration of 25 ns was directed to the target using a mirror. The nanoparticles generated through this method are pure, stable, and colloidal [45]. The de-cladded U-bent section of the fiber was immersed in the liquid containing the nanoparticles. The negative charges on the generated nanoparticles adhered to the amine functional group of the bonding agents and helped to form a layer of nanoparticles self-assembled on the surface of the optical fiber. After one hour, the fiber was carefully pulled out at a slow constant speed, yielding a uniform layer of nanoparticles on the silica glass. In the

case of Au + ZnO, Au nanoparticles were first synthesized, followed by ZnO nanoparticles. To measure the particle size and concentration, SEM images were acquired as shown in Figures 1–3. In each case, 70 nanoparticles were measured for the particle size distribution. The gold nanoparticles showed a narrow size distribution of  $5.7 \pm 1.7$  nm, while the ZnO nanoparticles showed a broader size distribution of  $38 \pm 19$  nm. The composite Au + ZnO nanoparticles showed a particle size distribution of  $42 \pm 17$  nm, similar to ZnO.

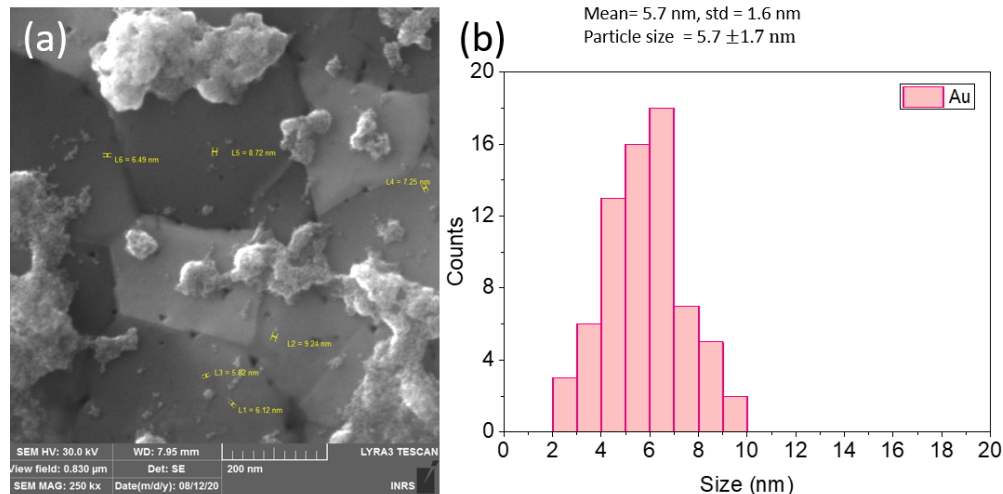


**Figure 1.** (a) SEM image and (b) particle size distribution of the Au nanoparticles grown by PLAL.

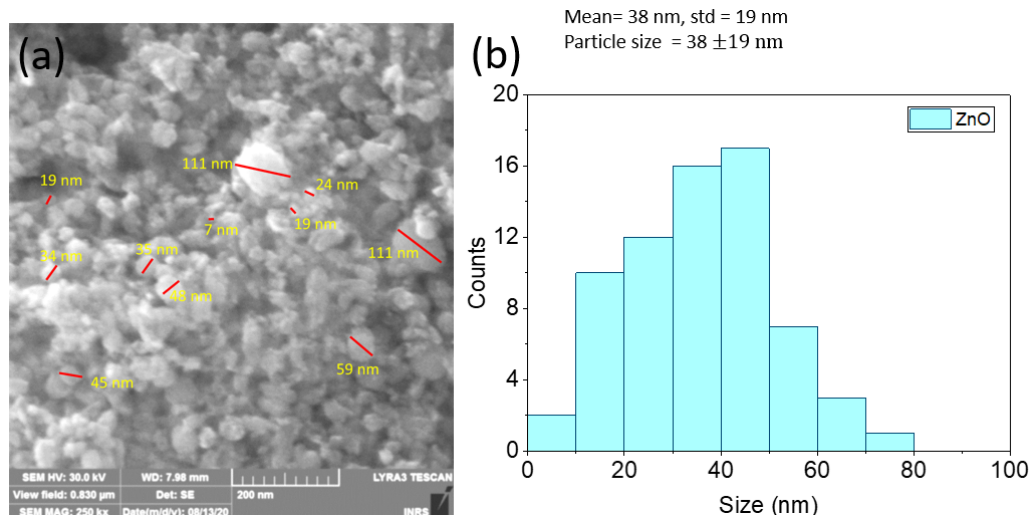


**Figure 2.** (a) SEM image and (b) particle size distribution of the ZnO nanoparticles grown by PLAL.

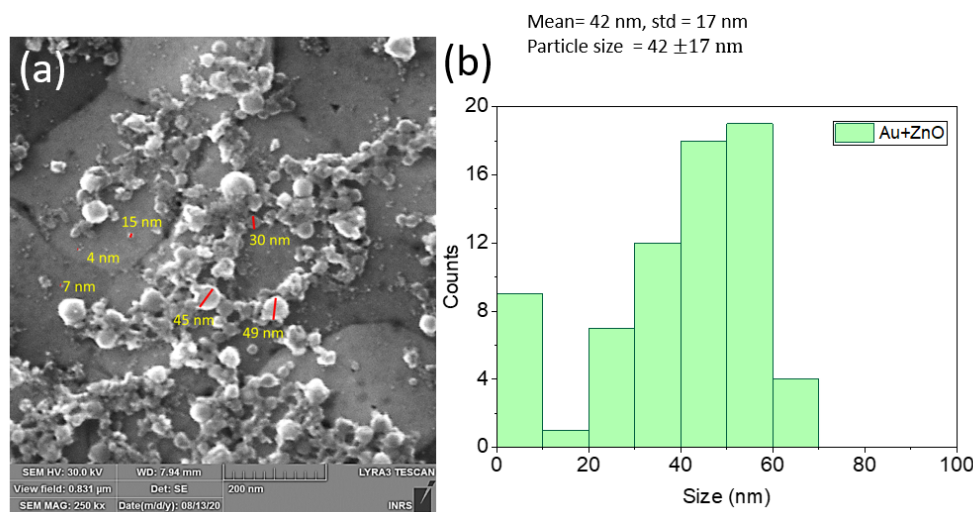


**Figure 3.** (a) SEM image and (b) particle size distribution of the Au + ZnO nanoparticles grown by PLAL.

The surface morphology of the deposited nanoparticles was imaged by AFM (Figures 4 and 5). The formation of the spherical islands of the nanoparticles was observed by visual inspection of the AFM images. Scanning along a sample line on the surface of a coated substrate re-demonstrated the Au particle size of  $4.9 \pm 0.9$  nm and ZnO particle size of  $39 \pm 8$  nm.

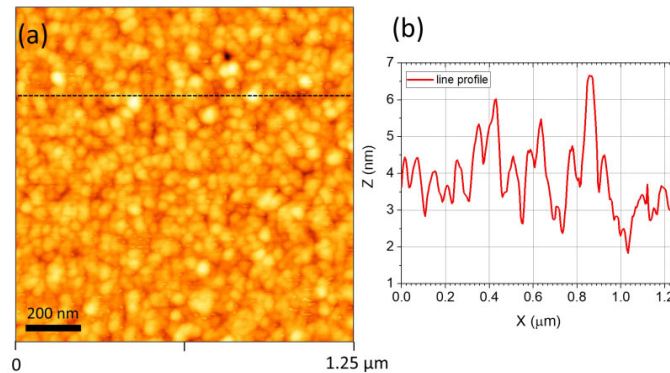


**Figure 4.** (a) AFM image of surface morphology and (b) line scan (across the dashed line) of the laser-ablated gold nanoparticle-coated U-bent optical fiber.

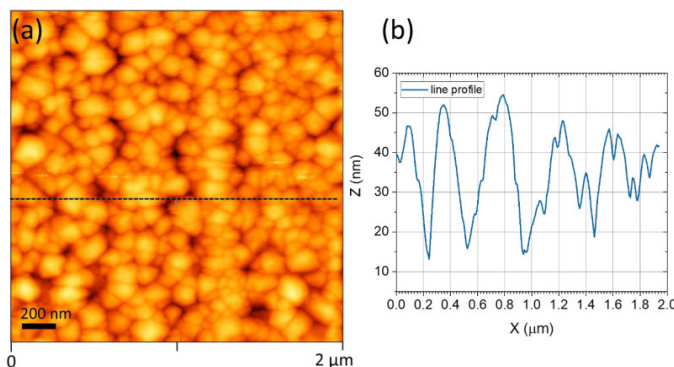


**Figure 5.** (a) AFM surface morphology and (b) line scan (across the dashed line) of the laser-ablated ZnO nanoparticle-coated U-bent optical fiber.

An X-ray diffraction (XRD) imaging was performed on Au nanoparticles to observe their crystallography. The XRD pattern is shown in Figure 6. The face-centered cubic lattice crystal structure demonstrated four peaks at XRD which represent standard Bragg reflections of (111), (200), (220), and (311) planes. The XRD pattern of ZnO nanoparticles has been previously reported in other works of this group [46–49].

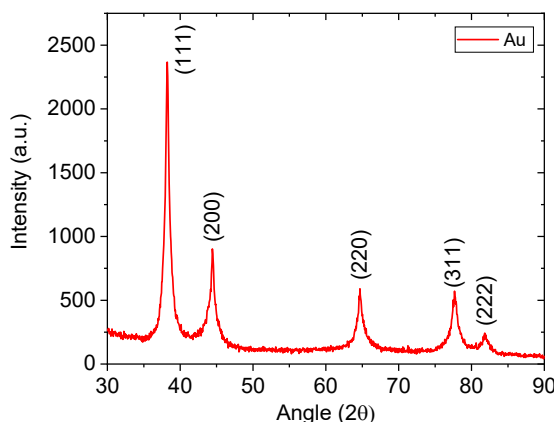


**Figure 6.** XRD Crystallite Size Calculator (Scherrer Equation) =  $11 \pm 2$  nm.

### 3.3. Thin Film Coating Using DC Magnetron Sputtering

Thin films of ZnO and ZnO + Au were deposited on the unclad section by magnetron sputtering on another set of uncoated U-bent fibers. In a magnetron sputtering, a metal target (ZnO and 1 or Au) is bombarded by Argon ions in an Ar plasma chamber, which results in the ejection of the target atoms. The ejected atoms then land on the sample surface. The film thickness was measured to be 18 nm and  $34 \text{ nm} \pm 2 \text{ nm}$ , respectively, by Scanning Electron Microscopy (SEM). Table 1 summarizes the characteristics of the materials coated on the fibers.

**Table 1.** Coating parameters.

Sample No.	Coating Method/Layer	Material	Film Thickness
1	Sputtering/thin film	ZnO	18 nm
2		ZnO + Au	$34 \text{ nm} \pm 2 \text{ nm}$
3		Au	$5.7 \pm 1.6 \text{ nm}$
4	PLAL/nanoparticles	ZnO	$38 \pm 19 \text{ nm}$
5		Au + ZnO	$42 \pm 17 \text{ nm}$

### 3.4. Test Setup

The fabricated probes were tested using a humidity chamber and an interrogation box developed by Maxwellian Inc., as shown in Figure 7a. The humidity chamber consists of a reference humidity sensor (TSP01 Thorlabs), a channel for introducing the room temperature water vapor, and a channel for introducing dry air into the chamber. The humidity chamber was controlled by a microcontroller system with reading feedback from the reference humidity sensor. The rising and falling cycles of the humidity chamber were monitored to ensure the reliability of the chamber. The humidity was set at 8 different points of 10–80% for a period of five minutes at each humidity level.

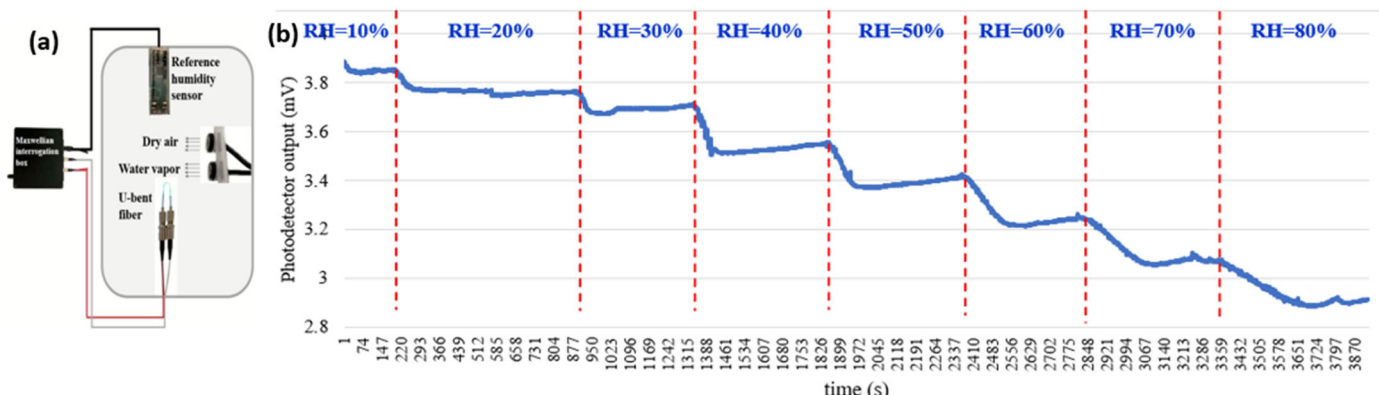


**Figure 7.** (a) Experimental setup to measure the response of the probes to the humidity. (b) A typical response of the probes to the humidity.

One end of the U-bent fiber was connected to a laser diode with a wavelength of 515 nm. This wavelength was selected based on the maximum absorbance of the Au nanoparticles, in order to supply the energy required to excite surface polaritons [50]. The laser was operated at an optical power of 2 mW and was pulsed at a frequency of 160 Hz and a pulse width of 1.78 ms. The laser diode light was modulated by pulse width modulation (PWM) at a specific frequency to avoid the effect of environmental noise of other frequencies on the optical reading. The other end of the U-bent fiber was connected to a photodetector synchronized with the laser pulse frequency. The output of the photodetector was amplified using a low-noise high-gain differential amplifier. The electrical circuit was specifically designed by Maxwellian Inc. to enable signal rerecording of >50 dB Signal to Noise Ratio (SNR). Experiments were performed to measure the stability of the photodetector output when the humidity was kept constant at 62% and 32%. To keep the humidity at a constant level, we used a Boveda 2-way humidity control package. The latter contains a saturated solution of salts in water that can naturally adjust the humidity to a pre-specified RH level in an enclosed chamber [51]. By monitoring the photodetector output for at least 24 h at a fixed input current of the laser, we observed that the output voltage had an average variation of 20  $\mu$ V. This 20  $\mu$ V was considered noise and removed from all the measured signals. Thus, only a change in the output voltage that was greater than 20  $\mu$ V was associated with a change in humidity. Figure 7b shows a typical response of the probes to the humidity. The slight increase of the output at a certain humidity corresponds to a slight loss of moisture during the five-minute period where the humidity was monitored and expected to be fixed at a value. The reference sensors were also calibrated using the commercial Boveda 2-way humidity-constant salts.

#### 4. Results and Discussion

The responses of the U-bent probes to humidity are reported in Figures 8 and 9, which show the normalized variation of the photodetector output power for fibers coated with the thin film layer and the fibers coated with the nanoparticles, respectively. The values were normalized to the response of the sensor at the minimum amount of the measured relative humidity (RH = 10%). The horizontal axis of the graphs represents the humidity measured by the reference sensor.

The results show that the output power decreases as humidity increases. The U-bent probes exploit the interaction of the water molecules in the air with the evanescent and surface polariton waves. Dry Au nanoparticles absorb in the 520–530 nm range [52]. Adding humidity increases the refractive index of air [53]. Therefore, when the humidity level increases, the surrounding refractive index is larger, which results in a larger portion of the optical power extending into the cladding region. The leaked power excites the polaritons, which are now in contact with the water molecules. This results in a lower

throughput power which translates into a lower signal at higher humidity. The same explanation is valid when the fiber is coated with the ZnO layer.

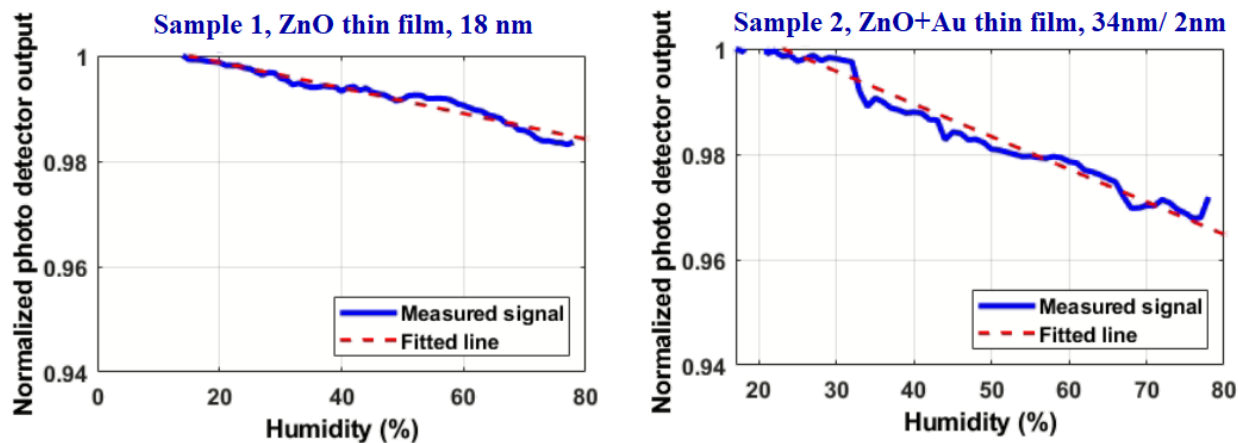


Figure 8. Response of the thin-film coated samples 1 (left) and 2 (right) to the change in humidity.

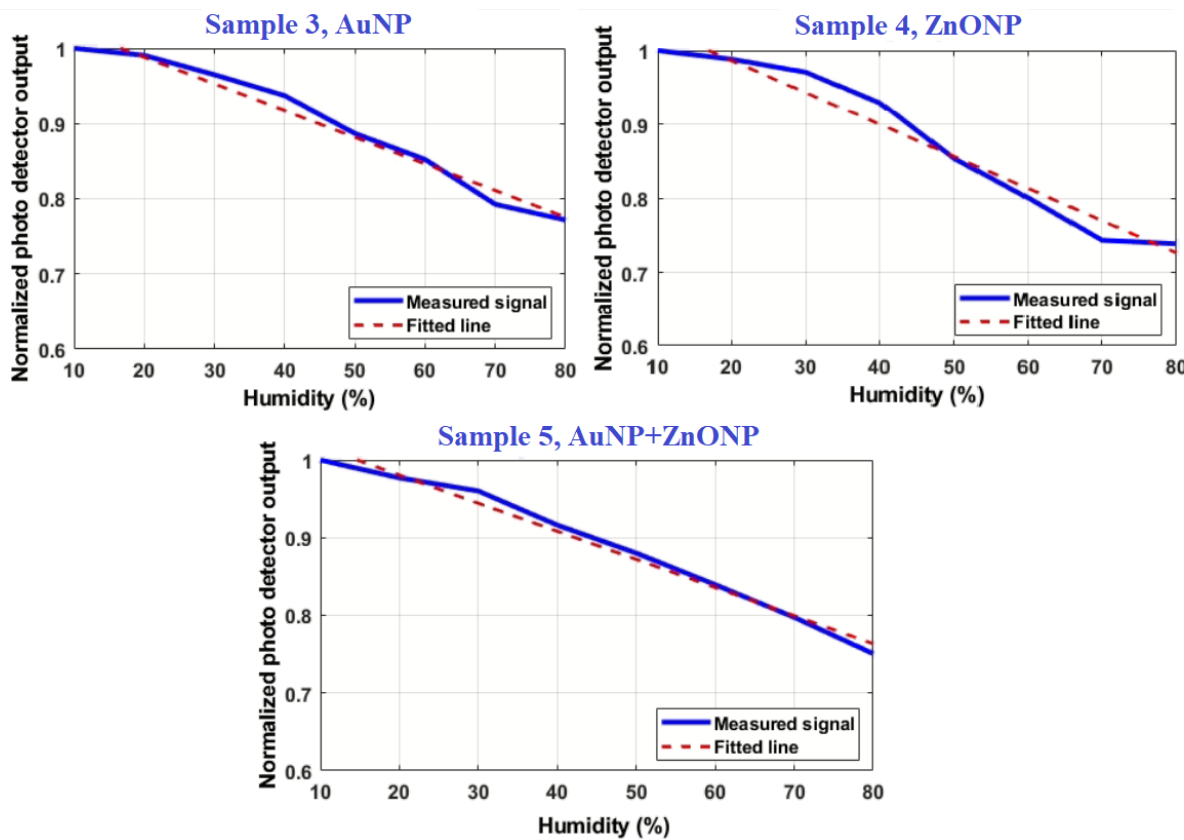


Figure 9. Response of the nanoparticle-coated samples 3 to 5 to the change in humidity. (NP: nanoparticles).

To better analyze the humidity graphs, the data shown in Figures 8 and 9 are summarized in Table 2. The sensitivity is defined as the fractional change in the output voltage per unit change in humidity. The minimum detectable humidity is calculated by dividing the minimum detectable voltage, after removing noise, ( $20 \mu\text{V}$ ) by the sensitivity ( $\mu\text{V}/\%\text{RH}$ ). The values in Table 2 show that the variation of the output power in the thin-film-coated probes is much less than for the probes coated with nanoparticles. This is mostly due to the denser layer of the sputtered ZnO + Au thin film compared to the nanoparticle-coated

samples. The density of the gold nanoparticles is reported to be  $19.32 \text{ g/cm}^3$  while the density of the ZnO nanoparticles is reported to be  $5.6 \text{ g/cm}^3$  [54]. In a more porous layer, the water molecules have a higher chance of bonding to the ZnO atoms, which results in a higher response to humidity. A denser film also features a higher refractive index. The higher refractive index of the ZnO thin film compared to the nanoparticles causes a larger fraction of light energy to be transferred to the ZnO thin film. Therefore, there is a large loss in the signal which results in a low response to humidity.

**Table 2.** Summary of the performance characteristics of the humidity probes.

Sample No.	Coating	Maximum Power Variation (%)	Linearity (%)	Sensitivity ( $\mu\text{V}/\%\text{RH}$ )	Minimum Detectable Humidity (%RH)
1	ZnO (18 nm)	1.7	0.94		Low sensitivity
2	ZnO + Au (34 nm + 2 nm)	3.0	0.91		
3	AuNp	29.9	0.97	71.6	0.3
4	ZnONp	38.9	0.95	143.6	0.1
5	Au + ZnO Nps	33.4	0.98	<20	2

In Samples 3–5 coated with nanoparticles, the responses to the humidity variation were observed to be between 29.9–33.4%, which was significantly larger than the responses of samples 1 and 2 (1.7–3%). For all the samples, the output power varied approximately linearly in the measured RH range.

The best sensitivity and resolution were observed for Sample 4, which was coated with ZnO nanoparticles. This sample demonstrated a sensitivity of  $143 \mu\text{V}/\%\text{RH}$ , with the capability to detect a 0.1% change in the humidity level. This observation can be explained by the intrinsically hydrophilic nature of ZnO, which has been shown to be due to the hydroxyl group existing at its surface [55]. In addition, the porosity of the deposited nanoparticles also helps to trap the water molecules as a second-order effect.

Sample 3, coated with Au nanoparticles, exhibited a sensitivity of  $71.6 \mu\text{V}/\%\text{RH}$  with a humidity detection resolution of 0.3%. The sensing mechanism in this type of coating is mostly based on the optically excited localized surface plasmons confined at the interface of the AuNP and the fiber core.

Sample 5, which was coated with the composite of Au + ZnO nanoparticles, had a lower sensitivity to humidity. The minimum detectable humidity using the Au + ZnO nanoparticle-coated samples is 2%. This is attributed to the larger number of nanoparticles per unit area on the fibers coated with the composite of Au + ZnO nanoparticles compared to the fibers coated with either AuNp or ZnONp. In a denser layer, the particles have a lower chance of bonding to water molecules, since their open ends are already bonded to the surrounding atoms.

Figure 10 exhibits the response of a ZnO nanoparticle-coated fiber to a sudden change in humidity from 20% to 80% and then reversed. The rising time and the falling time have been enlarged. The 60% rise in humidity can be detected in 3 s while a one percent change in the humidity can be detected in 50 ms. When humidity is dropped to the initial value of 20%, it takes approximately 4 s for the sensor to reach its final detection level, which yields a 67 ms per %RH recovery time of the sensor.

Table 3 summarizes the performance of seven evanescent wave humidity sensors reported in the literature. Assuming that the geometry and the operating wavelength were optimized for all the experiments, it can be concluded from Table 3 that the efficiency of an evanescent wave humidity sensor strongly depends on its coating. Each coating material has some advantages and some drawbacks. For example, the U-bent fiber described in reference [30] was coated with PVA as a sensing agent and was able to detect a change in humidity as low as 0.0629% RH. Another successful example of using PVA as a sensing

agent was reported by Khijiwania et al. [21]. In [21] the PVA film was doped with  $\text{CoCl}_2$  which resulted in very high sensitivity and a large dynamic range. However, according to [32], the PVA film dries off at RH values of around 50%, which makes it insensible to further humidity drops. The authors suggested using Agarose which is a polysaccharide polymer. At the 1600 nm wavelength, the sensor demonstrated the highest response to the humidity, with a very fast response speed of 50 ms [32]. Co [37] and MgO [34] nanoparticles also demonstrated a high sensitivity to humidity, but not a fast response time. Fibers coated with silica doped with Methylene Blue could also detect a very low change in humidity. However, they suffer from a relatively slow response time of 20 s and a recovery time of 180 s [31].

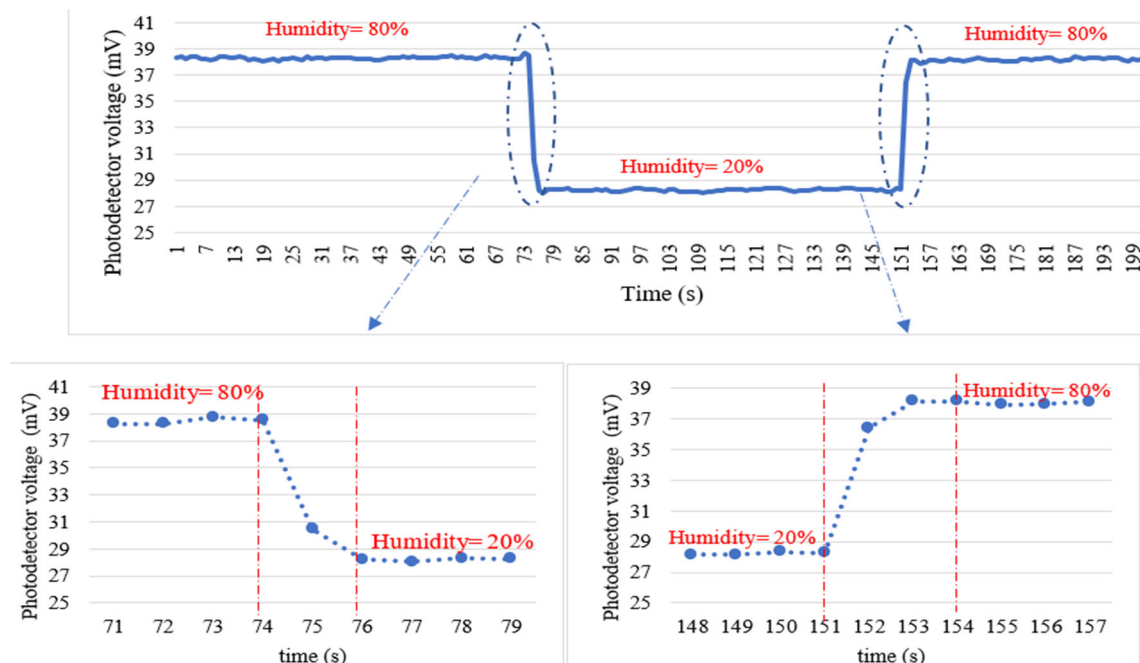


**Figure 10.** Response of the U-bent fiber coated with the ZnO nanoparticles to a sudden change in humidity.

**Table 3.** Humidity sensors working based on the evanescent-wave surface plasmon excitation principle reported in the literature.

Reference	Coating Material	Mechanism	Humidity Range	Sensitivity	Resolution	Linearity	Response Time	Strength Point
Y. Zhao et al. [30]	PVA	EW, U-bent probe, Wavelength variation	15–85%	318.1 pm/%RH	0.0629% RH	99%	NF	Excellent resolution
A. Vijayan et al. [37]	Co nanoparticles dispersed in polyaniline	EW, U-bent Optical power variation	20–100%	2 mV/%RH (between 35% to 80%)	NF	NF	8 s rise/60 s fall	High sensitivity in a wide range
Z. Zhao et al. [31]	Silica doped with Methylene Blue	EW, U-bent Optical power variation	1.1–70%	0.087 dB/%RH (between 1.1% to 4.1%)	0.062% RH (between 1.1% to 4.1%)	logarithmic	20 s rise/180 s fall	Excellent resolution

**Table 3.** Cont.

Reference	Coating Material	Mechanism	Humidity Range	Sensitivity	Resolution	Linearity	Response Time	Strength Point
S. K. Shukla et al. [34]	MgO	EW, U-bent Optical power variation	5–80%	(0.037–0.015)/75 (W) 0.3 mW/%RH	NF	NF	NF	High sensitivity
J. Mathew et al. [32]	Agarose	EW, U-bent Optical power variation/wavelength optimized	25–90%	100 mDB/%RH at 1600 nm wavelength	NF	Linear	50 ms rise/700 ms fall (60–90%)	High sensitivity, fast response, and recovery time
S. Khijwania et al. [21]	PVA dopped with CoCl <sub>2</sub>	EW, U-bent, Optical power variation/	10–90%	27 mV/%RH	NF	Linear	1 s	Very high sensitivity
This work	ZnO nanoparticles	EW excited surface polaritons	10–80%	143 $\mu$ V/%RH	0.1% RH	95% in the whole range	3 s rise/4 s fall (20–80%)	Very good resolution, Linear, Fast response, and recovery time

EW: Evanescent Wave; NF: Not Found; RH: Relative Humidity.

Compared to the evanescent field-based humidity sensors reported by other groups, we conclude that the U-bent fiber presented herein constitutes a fair trade-off between an acceptable sensitivity (143  $\mu$ V/%RH), a very good resolution of detecting 0.1% change in humidity, and a fast response and recovery time of 50–67 ms/%RH. Since the sensor setup is designed to be portable and compatible to operate with 12 V batteries, this device offers accurate measurement of humidity in real-life conditions.

## 5. Conclusions and Perspectives

We describe the design and realization of a fiber optics-based evanescent-wave humidity sensor. The sensing mechanism is based on the excitation of the surface polaritons at the interface between the Au/ZnO nanoparticles and the uncladded U-shaped section of the silica fiber. We developed two types of coating, specifically, thin films and nanoparticles, and observed that the response to humidity variation was stronger for the fibers coated with nanoparticles. To improve the bonding of the nanoparticles to silica, the surface was salinized using APTMS. The fiber coated with ZnO nanoparticles demonstrated a humidity detection sensitivity of 143  $\mu$ V/%RH, with a resolution of 0.1% RH. The response to the humidity change was 95% linear in the 10–80% humidity range. The response and recovery time of the sensor to a 60% change in humidity (20 to 80%) were measured to be 3 s and 4 s, respectively, which corresponds to a response time of 50–67 ms/%RH. Compared to its counterparts presented in Table 3, the sensor reported herein features very good resolution, high linearity over a wide range, and fast response and recovery time. These results were obtained by using the interrogation box developed by Maxwellian Inc., which performed the tasks of driving the laser diode, reading out from the photodetector, and transferring the data to the user interface while consuming 1.62 W of electrical power at a dc voltage of 12 V. This feature allows the sensor system to be portable and functional in real practical environments.

**Author Contributions:** Conceptualization, A.H.; methodology, A.H., K.D.M. and M.M.; software, E.A. and R.S.; validation, E.A., M.M. and E.M.; formal analysis, E.A.; investigation, A.H., E.A., M.M. and E.M.; resources, A.H., M.C. and F.R.; data curation, R.S.; writing—original draft preparation, E.A.; writing—review and editing, M.C. and F.R.; visualization, E.A. and K.D.M.; supervision, F.R. and M.C.; project administration, F.R., M.C. and A.H.; funding acquisition, F.R., M.C. and A.H. All authors have read and agreed to the published version of the manuscript.

**Funding:** This research was funded by Maxwellian Inc., Natural Sciences and Engineering Research Council (NSERC), and the MITACS Accelerate program with fund number IT21950.

**Data Availability Statement:** Not applicable.

**Acknowledgments:** F.R. is grateful to the Canada Research Chairs program for partial salary support.

**Conflicts of Interest:** The authors declare no conflict of interest.

## References

1. Yang, W.; Marr, L.C. Mechanisms by Which Ambient Humidity May Affect Viruses in Aerosols. *Appl. Environ. Microbiol.* **2012**, *78*, 6781–6788. [[CrossRef](#)] [[PubMed](#)]
2. Peinado, A.; Hammond, J.; Scott, A. Development, validation and transfer of a Near Infrared method to determine in-line the end point of a fluidised drying process for commercial production batches of an approved oral solid dose pharmaceutical product. *J. Pharm. Biomed. Anal.* **2011**, *54*, 13–20. [[CrossRef](#)] [[PubMed](#)]
3. Arimi, J.; Duggan, E.; O’Sullivan, M.; Lyng, J.; O’Riordan, E. Effect of moisture content and water mobility on microwave expansion of imitation cheese. *Food Chem.* **2010**, *121*, 509–516. [[CrossRef](#)]
4. Dijkink, B.H.; Tomassen, M.M.; Willemse, J.H.; van Doorn, W.G. Humidity control during bell pepper storage, using a hollow fiber membrane contactor system. *Postharvest Biol. Technol.* **2004**, *32*, 311–320. [[CrossRef](#)]
5. Sberveglieri, G.; Rinchetti, G.; Groppelli, S.; Faglia, G. Capacitive humidity sensor with controlled performances, based on porous Al<sub>2</sub>O<sub>3</sub> thin film grown on SiO<sub>2</sub>-Si substrate. *Sens. Actuators B Chem.* **1994**, *19*, 551–553. [[CrossRef](#)]
6. Anchisini, R.; Faglia, G.; Gallazzi, M.; Sberveglieri, G.; Zerbi, G. Polyphosphazene membrane as a very sensitive resistive and capacitive humidity sensor. *Sens. Actuators B Chem.* **1996**, *35*, 99–102. [[CrossRef](#)]
7. Ali, S.; Jameel, M.A.; Harrison, C.J.; Gupta, A.; Shafiei, M.; Langford, S.J. Nanoporous naphthalene diimide surface enhances humidity and ammonia sensing at room temperature. *Sens. Actuators B Chem.* **2021**, *351*, 130972. [[CrossRef](#)]
8. Ali, S.; Jameel, M.A.; Harrison, C.J.; Gupta, A.; Evans, R.A.; Shafiei, M.; Langford, S.J. Enhanced Capacitive Humidity Sensing Performance at Room Temperature via Hydrogen Bonding of Cyanopyridone-Based Oligothiophene Donor. *Chemosensors* **2021**, *9*, 320. [[CrossRef](#)]
9. Farahani, H.; Wagiran, R.; Hamidon, M.N. Humidity Sensors Principle, Mechanism, and Fabrication Technologies: A Comprehensive Review. *Sensors* **2014**, *14*, 7881–7939. [[CrossRef](#)]
10. Mogera, U.; Sagade, A.A.; George, S.J.; Kulkarni, G.U. Ultrafast response humidity sensor using supramolecular nanofibre and its application in monitoring breath humidity and flow. *Sci. Rep.* **2014**, *4*, 4103. [[CrossRef](#)]
11. Borini, S.; White, R.; Wei, D.; Astley, M.; Haque, S.; Spigone, E.; Harris, N.; Kivioja, J.; Ryhänen, T. Ultrafast Graphene Oxide Humidity Sensors. *ACS Nano* **2013**, *7*, 11166–11173. [[CrossRef](#)] [[PubMed](#)]
12. Rao, X.; Zhao, L.; Xu, L.; Wang, Y.; Liu, K.; Wang, Y.; Chen, G.Y.; Liu, T.; Wang, Y. Review of Optical Humidity Sensors. *Sensors* **2021**, *21*, 8049. [[CrossRef](#)] [[PubMed](#)]
13. Alwis, L.; Sun, T.; Grattan, K.T.V. Optical fibre-based sensor technology for humidity and moisture measurement: Review of recent progress. *Measurement* **2013**, *46*, 4052–4074. [[CrossRef](#)]
14. Sikarwar, S.; Yadav, B.C. Opto-electronic humidity sensor: A review. *Sens. Actuators A Phys.* **2015**, *233*, 54–70. [[CrossRef](#)]
15. Estella, J.; de Vicente, P.; Echeverría, J.C.; Garrido, J.J. A fibre-optic humidity sensor based on a porous silica xerogel film as the sensing element. *Sens. Actuators B Chem.* **2010**, *149*, 122–128. [[CrossRef](#)]
16. Wang, B.; Zhang, F.; Pang, F.; Wang, T. An optical fiber humidity sensor based on optical absorption. *Opt. Sens. Biophotonics* **2011**, vol. 8311, 83112A. [[CrossRef](#)]
17. Kronenberg, P.; Rastogi, P.K.; Giaccari, P.; Limberger, H.G. Relative humidity sensor with optical fiber Bragg gratings. *Opt. Lett.* **2002**, *27*, 1385–1387. [[CrossRef](#)]
18. Berruti, G.; Consales, M.; Giordano, M.; Sansone, L.; Petagna, P.; Buontempo, S.; Breglio, G.; Cusano, A. Radiation hard humidity sensors for high energy physics applications using polyimide-coated fiber Bragg gratings sensors. *Sens. Actuators B Chem.* **2013**, *177*, 94–102. [[CrossRef](#)]
19. Yeo, T.; Sun, T.; Grattan, K.; Parry, D.; Lade, R.; Powell, B. Polymer-coated fiber Bragg grating for relative humidity sensing. *IEEE Sens. J.* **2005**, *5*, 1082–1089. [[CrossRef](#)]
20. Chen, L.; Li, T.; Chan, C.; Menon, R.; Balamurali, P.; Shaillender, M.; Neu, B.; Ang, X.; Zu, P.; Wong, W.; et al. Chitosan based fiber-optic Fabry–Perot humidity sensor. *Sens. Actuators B Chem.* **2012**, *169*, 167–172. [[CrossRef](#)]
21. Khijwania, S.K.; Srinivasan, K.L.; Singh, J.P. An evanescent-wave optical fiber relative humidity sensor with enhanced sensitivity. *Sens. Actuators B Chem.* **2005**, *104*, 217–222. [[CrossRef](#)]

22. Matias, I.R.; Arregui, F.J.; Corres, J.M.; Bravo, J. Evanescent Field Fiber-Optic Sensors for Humidity Monitoring Based on Nanocoatings. *IEEE Sens. J.* **2006**, *7*, 89–95. [[CrossRef](#)]
23. Satija, J.; Punjabi, N.; Sai, V.V.R.; Mukherji, S. Optimal Design for U-bent Fiber-optic LSPR Sensor Probes. *Plasmonics* **2014**, *9*, 251–260. [[CrossRef](#)]
24. Ramakrishna, B.; Sai, V. Evanescent wave absorbance based U-bent fiber probe for immunobiosensor with gold nanoparticle labels. *Sens. Actuators B Chem.* **2016**, *226*, 184–190. [[CrossRef](#)]
25. Zhang, C.; Li, Z.; Jiang, S.Z.; Li, C.H.; Xu, S.C.; Yu, J.; Wang, M.H.; Liu, A.H.; Man, B.Y. U-bent fiber optic SPR sensor based on graphene/AgNPs. *Sens. Actuators B Chem.* **2017**, *251*, 127–133. [[CrossRef](#)]
26. Takagi, K.; Sasaki, H.; Seki, A.; Watanabe, K. Surface plasmon resonances of a curved hetero-core optical fiber sensor. *Sens. Actuators A Phys.* **2010**, *161*, 1–5. [[CrossRef](#)]
27. Rivero, P.J.; Urrutia, A.; Goicoechea, J.; Arregui, F. Optical fiber humidity sensors based on Localized Surface Plasmon Resonance (LSPR) and Lossy-mode resonance (LMR) in overlays loaded with silver nanoparticles. *Sens. Actuators B Chem.* **2012**, *173*, 244–249. [[CrossRef](#)]
28. Lin, J.; Tanada, H.; Odawara, K.; Hiragino, Y.; Fujita, Y. Localized Surface Plasmon Effect for ZnO Nanoparticles Based Devices. JSAP-OSA Joint Symposia, Washington, DC, USA; 2015. Available online: [https://www.osapublishing.org/abstract.cfm?uri=JSAP-2015-13a\\_2C\\_4](https://www.osapublishing.org/abstract.cfm?uri=JSAP-2015-13a_2C_4) (accessed on 1 May 2021).
29. Mei, G.S.; Menon, P.S.; Hegde, G. ZnO for performance enhancement of surface plasmon resonance biosensor: A review. *Mater. Res. Express* **2020**, *7*, 012003. [[CrossRef](#)]
30. Zhao, Y.; Peng, Y.; Chen, M.-Q.; Xia, F.; Tong, R.-J. U-shaped microfiber coupler coated with polyvinyl alcohol film for highly sensitive humidity detection. *Sens. Actuators A Phys.* **2019**, *285*, 628–636. [[CrossRef](#)]
31. Zhao, Z.; Duan, Y. A low cost fiber-optic humidity sensor based on silica sol–gel film. *Sens. Actuators B Chem.* **2011**, *160*, 1340–1345. [[CrossRef](#)]
32. Mathew, J.; Semenova, Y.; Farrell, G. A fiber bend based humidity sensor with a wide linear range and fast measurement speed. *Sens. Actuators A Phys.* **2012**, *174*, 47–51. [[CrossRef](#)]
33. Yadav, B.C.; Shukla, R.K.; Bali, L.M. Sol-gel processed TiO<sub>2</sub> films on U-shaped glass-rods as optical humidity sensor. *Indian J. Pure Appl. Phys.* **2005**, *43*, 51–55.
34. Shukla, S.; Parashar, G.; Mishra, A.; Misra, P.; Yadav, B.; Bali, L.; Dubey, G. Nano-like magnesium oxide films and its significance in optical fiber humidity sensor. *Sens. Actuators B Chem.* **2004**, *98*, 5–11. [[CrossRef](#)]
35. Fuke, M.V.; Kanitkar, P.; Kulkarni, M.; Kale, B.; Aiyer, R. Effect of particle size variation of Ag nanoparticles in Polyaniline composite on humidity sensing. *Talanta* **2010**, *81*, 320–326. [[CrossRef](#)] [[PubMed](#)]
36. Gupta, B.; Ratnanjali. A novel probe for a fiber optic humidity sensor. *Sens. Actuators B Chem.* **2001**, *80*, 132–135. [[CrossRef](#)]
37. Vijayan, A.; Fuke, M.; Hawaldar, R.; Kulkarni, M.; Amalnerkar, D.; Aiyer, R. Optical fibre based humidity sensor using Co-polyaniline clad. *Sens. Actuators B Chem.* **2008**, *129*, 106–112. [[CrossRef](#)]
38. Zamarreño, C.; Hernaez, M.; Del Villar, I.; Matias, I.; Arregui, F. Tunable humidity sensor based on ITO-coated optical fiber. *Sens. Actuators B Chem.* **2010**, *146*, 414–417. [[CrossRef](#)]
39. Paul, D.; Dutta, S.; Saha, D.; Biswas, R. LSPR based Ultra-sensitive low cost U-bent optical fiber for volatile liquid sensing. *Sens. Actuators B Chem.* **2017**, *250*, 198–207. [[CrossRef](#)]
40. Gao, S.S.; Qiu, H.W.; Zhang, C.; Jiang, S.Z.; Li, Z.; Liu, X.Y.; Yue, W.W.; Yang, C.; Huo, Y.Y.; Feng, D.J.; et al. Absorbance response of a graphene oxide coated U-bent optical fiber sensor for aqueous ethanol detection. *RSC Adv.* **2016**, *6*, 15808–15815. [[CrossRef](#)]
41. Xiong, F.; Sisler, D. Determination of low-level water content in ethanol by fiber-optic evanescent absorption sensor. *Opt. Commun.* **2010**, *283*, 1326–1330. [[CrossRef](#)]
42. Fabian, M.; Lewis, E.; Newe, T.; Lochmann, S.; Mueller, I. Investigation of ethanol and methanol water mixtures in the visible wavelength area using fibre-optic evanescent field absorption sensors based on a u-shaped, a coil-shaped and a meander-shaped probe. In Proceedings of the 2008 IEEE Sensors Applications Symposium, SAS-2008—Proceedings, Atlanta, GA, USA, 12–14 February 2008; pp. 79–84. [[CrossRef](#)]
43. Memon, S.F.; Ali, M.M.; Pembroke, J.T.; Chowdhry, B.S.; Lewis, E. Measurement of Ultralow Level Bioethanol Concentration for Production Using Evanescent Wave Based Optical Fiber Sensor. *IEEE Trans. Instrum. Meas.* **2017**, *67*, 780–788. [[CrossRef](#)]
44. Cai, H.; Chu, F.; Qu, R. U-shaped plastic optical fiber dissolved oxygen sensor. In Proceedings of the 19th International Conference on Optical Fibre Sensors, Perth, Australia, 15–18 April 2008; Volume 7004, p. 70042B. [[CrossRef](#)]
45. Tri, P.N.; Ouellet-Plamondon, C.; Rtimi, S.; Assadi, A.A.; Nguyen, T.A. Chapter 3—Methods for Synthesis of Hybrid Nanoparticles. In *Noble Metal-Metal Oxide Hybrid Nanoparticles*; Mohapatra, S., Nguyen, T.A., Nguyen-Tri, P., Eds.; Woodhead Publishing: Sawston, UK, 2019; pp. 51–63. [[CrossRef](#)]
46. Mohammadnezhad, M.; Aïssa, B.; Harnagea, C.; Bentouaf, A.; Haddad, E.; Rosei, F. Photovoltaic properties of hybrid c-Si/ZnO nanorod solar cells. *Mater. Adv.* **2022**, *3*, 5911–5921. [[CrossRef](#)]
47. Henni, A.; Harfouche, N.; Karar, A.; Zerrouki, D.; Perrin, F.; Rosei, F. Synthesis of graphene–ZnO nanocomposites by a one-step electrochemical deposition for efficient photocatalytic degradation of organic pollutant. *Solid State Sci.* **2019**, *98*, 106039. [[CrossRef](#)]
48. Selloum, D.; Henni, A.; Karar, A.; Tabchouche, A.; Harfouche, N.; Bacha, O.; Tingry, S.; Rosei, F. Effects of Fe concentration on properties of ZnO nanostructures and their application to photocurrent generation. *Solid State Sci.* **2019**, *92*, 76–80. [[CrossRef](#)]

49. Papadaki, D.; Mhlongo, G.H.; Motaung, D.E.; Nkosi, S.S.; Panagiotaki, K.; Christaki, E.; Assimakopoulos, M.N.; Papadimitriou, V.C.; Rosei, F.; Kiriakidis, G.; et al. Hierarchically Porous Cu-, Co-, and Mn-Doped Platelet-Like ZnO Nanostructures and Their Photocatalytic Performance for Indoor Air Quality Control. *ACS Omega* **2019**, *4*, 16429–16440. [[CrossRef](#)]
50. Selopal, G.S.; Mohammadnezhad, M.; Besteiro, L.V.; Cavuslar, O.; Liu, J.; Zhang, H.; Navarro-Pardo, F.; Liu, G.; Wang, M.; Durmusoglu, E.G.; et al. Synergistic Effect of Plasmonic Gold Nanoparticles Decorated Carbon Nanotubes in Quantum Dots/TiO<sub>2</sub> for Optoelectronic Devices. *Adv. Sci.* **2020**, *7*, 2001864. [[CrossRef](#)]
51. Cited, R.; Springs, B.; Esse, R.L. Humidity Control System for Wood Products. U.S. Patent US8748723B1, 10 June 2014.
52. He, Y.Q.; Liu, S.P.; Kong, L.; Liu, Z.F. A study on the sizes and concentrations of gold nanoparticles by spectra of absorption, resonance Rayleigh scattering and resonance non-linear scattering. *Spectrochim. Acta Part A Mol. Biomol. Spectrosc.* **2005**, *61*, 2861–2866. [[CrossRef](#)]
53. Birch, K.P.; Downs, M.J. The results of a comparison between calculated and measured values of the refractive index of air. *J. Phys. E Sci. Instrum.* **1988**, *21*, 694–695. [[CrossRef](#)]
54. Uekey, P.; Vishwakarma, K. Review of zinc oxide (ZnO) nanoparticles applications and properties. *J. Emerg. Technol. Comput. Sci. Electron.* **2016**, *21*, 239–242.
55. Ennaceri, H.; Wang, L.; Erfurt, D.; Riedel, W.; Mangalgiri, G.; Khaldoun, A.; El Kenz, A.; Benyoussef, A.; Ennaoui, A. Water-resistant surfaces using zinc oxide structured nanorod arrays with switchable wetting property. *Surf. Coat. Technol.* **2016**, *299*, 169–176. [[CrossRef](#)]

**Disclaimer/Publisher's Note:** The statements, opinions and data contained in all publications are solely those of the individual author(s) and contributor(s) and not of MDPI and/or the editor(s). MDPI and/or the editor(s) disclaim responsibility for any injury to people or property resulting from any ideas, methods, instructions or products referred to in the content.